A mechanism study of sound wave-trapping barriers ⊘

Cheng Yang; Jie Pan; Li Cheng

🔴 Check for updates

🌐 View Online

📄 Export Citation

A mechanism study of sound wave-trapping barriers

Cheng Yang

Mechanical Engineering Department, The Hong Kong Polytechnic University, Hung Hom, Hong Kong, SAR China

Jie Pan[a)]

School of Mechanical and Chemical Engineering, The University of Western Australia, 35 Stirling Highway, Crawley, Western Australia 6009, Australia

Li Cheng

Mechanical Engineering Department, The Hong Kong Polytechnic University, Hung Hom, Hong Kong, SAR China

The performance of a sound barrier is usually degraded if a large reflecting surface is placed on the source side. A wave-trapping barrier (WTB), with its inner surface covered by wedge-shaped structures, has been proposed to confine waves within the area between the barrier and the reflecting surface, and thus improve the performance. In this paper, the deterioration in performance of a conventional sound barrier due to the reflecting surface is first explained in terms of the resonance effect of the trapped modes. At each resonance frequency, a strong and mode-controlled sound field is generated by the noise source both within and in the vicinity outside the region bounded by the sound barrier and the reflecting surface. It is found that the peak sound pressures in the barrier's shadow zone, which correspond to the minimum values in the barrier's insertion loss, are largely determined by the resonance frequencies and by the shapes and losses of the trapped modes. These peak pressures usually result in high sound intensity component impinging normal to the barrier surface near the top. The WTB can alter the sound wave diffraction at the top of the barrier if the wavelengths of the sound wave are comparable or smaller than the dimensions of the wedge. In this case, the modified barrier profile is capable of re-organizing the pressure distribution within the bounded domain and altering the acoustic properties near the top of the sound barrier.
© 2013 Acoustical Society of America. [http://dx.doi.org/10.1121/1.4816542]

I. INTRODUCTION

A sound barrier is the most commonly used structure for solving environmental noise problems. Its applications are widely seen in many outdoor engineering projects, such as highways,[1] railways,[2] and high-rise buildings.[3] In general, a sound barrier is placed between the noise source and the receiver to prevent the sound wave from directly approaching the receiver.

Behind the barrier and on the receiver side, a shadow zone exists where only the waves diffracted by the barrier top can arrive. To characterize the diffraction field, Keller[4] developed the geometrical theory of diffraction (GTD), showing that the source of the diffracted rays is determined by the incident rays toward the barrier's top and by an appropriate diffraction coefficient. The diffraction coefficient is dependent on the directions of incidence and diffraction, the wavelength, and the geometrical and physical properties of the media at the point of diffraction.

In this spirit, Pierce[5] proposed an analytical model to predict the sound pressure diffracted by a wedge. On the other hand, Maekawa[6] gave an empirical formula based on extensive experimental measurements to estimate sound barrier performance. This formula is easy to use and has become a rough design tool in a wide range of noise

abatement engineering projects. A myriad of works regarding the use of sound barriers to reduce environmental noise are available in the literature; some good reviews of these studies have been given by Ekici and Bougdah[7] and Li and Wong.[8]

To improve the performance of the sound barriers in attenuating incoming noise, barriers with new profiles, such as circular, *T*-shaped, *Y*-shaped, and branched, have been designed.[9–12] However, a problem arose with these new types of barriers in that the conventional analytical and empirical methods are no longer capable of dealing with barriers with complex profiles. In this regard, the boundary element method (BEM)[13–15] becomes a good option for studying the performance of a sound barrier with complex profiles. By discretely solving the boundary integral equations via the BEM, acoustic quantities (such as pressure and air particle velocity) can be readily obtained. The basic formulation and implementation of a collocation BEM are well established.[16] However, errors may arise when performing discretization and solving integrations. A discussion of the errors occurring in the direct collocation BEM was presented by Treeby and Pan,[17] and an empirical guideline to maintain a given global error constraint was suggested.

The performance of a sound barrier may be significantly deteriorated when a large reflecting surface is placed on the source side, in which case multiple reflections occur between the barrier and the reflecting surface.[18,19] Watts[20] showed in an experimental study that multiple reflections significantly

---
[a)]Author to whom correspondence should be addressed. Electronic mail: jie.pan@uwa.edu.au

degraded barrier performance. In his study, the insertion loss (IL) of a sound barrier with a 2 m height was reduced by 4 dB(A) if a reflecting wall of the same height was erected on the source side. As a solution, it was suggested to use absorption material or a tilted barrier to reduce this deterioration. Monazzam and Fard[21] studied the use of different shapes of sound barrier to reduce the deterioration. Their comparison suggested that a tilted barrier with a 10° slope yielded the best IL. Indeed, the tilted barrier redirects the sound wave upward, which reduces diffraction at the barrier top.

On the same principle, Pan et al.[22] proposed a wave-trapping barrier (WTB). The WTB has a profile with multiple wedges on its surface. Each wedge has a perforated surface, a back cavity, and internal lining to provide appropriate reflection and absorption of incident sound waves. The qualitative interpretation of a WTB is that the wedges always redirect reflected waves downwards to the ground so that they are trapped within the domain bounded by the barrier and reflecting surface. The superiority of the WTB over conventional sound barriers has been experimentally validated at the Willowdale mining site in Western Australia.

In parallel with this development, Fahy et al.[23] experimentally examined a sound barrier with a wedged profile. In their model, the wedge was coated by an absorption material and the sloping wedge deflected the sound wave upward. The field test[22] and scale model test[23] demonstrated the potential of using a surface profile and sound absorption on the sound barrier surface to overcome the performance degradation due to multiple reflections. These previous experimental works also demonstrated the need for understanding how the multiple reflections degrade the barrier performance and how exactly the surface profile and absorption affect the sound reflection between the barrier and reflecting surface and the diffraction of sound at the barrier top.

The main function of a sound barrier is shielding the receiver region within a shadow zone. Since only the diffracting waves can arrive in this region, the acoustic properties at the barrier top, i.e., the diffracting point, are crucial to the performance of the barrier.[4,5,24] When the incident sound wave approaches the barrier top, the scattered sound field at the barrier top becomes a secondary source. This secondary source then radiates sound waves in all directions. When multiple diffractions take place, the resulting sound pressure can be solved iteratively.[25–27] Without the reflecting surface, the acoustic properties of the secondary source can be easily obtained from the direct wave and the reflecting wave from the ground.

If a reflecting surface is present, then a large number of reflections and diffractions will occur for the waves between the barrier and the reflecting surface. If the acoustical domain is enclosed by boundaries, then the sound field within the domain can be obtained by the superposition of acoustical modes.[28] These modes, in turn, are determined by the geometry of the domain and the properties of the boundaries. A question is then posed when an acoustical space confined by two barriers is connected with an infinite space: "Is the sound field in the sound barrier configuration contributed to by any acoustical modes?" This paper will reveal the existence of these acoustical modes, as a set of trapped modes, and the

mechanism of sound scattering of these modes at the barrier top in relation to the decreased IL of a sound barrier with a large reflecting surface on the source side. Furthermore, the improvement of the IL when a WTB is used is explained by the changes in the sound scattering characteristics of the resultant modes at the barrier top.

II. MODELING OF THE SOUND BARRIERS

Figure 1(a) shows the cross sections (in the x-y plane) of sound barriers with various surface profiles erected on the ground. It is assumed that: (1) The cross sections are unchanged in the z-direction, and (2) a harmonic time-dependence sound pressure field is generated by a line source at (x_s, y_s) in the cross-section plane. The sound pressure field can then be described by a two-dimensional inhomogeneous Helmholtz equation:

$$\nabla^2 p(x, y) + k^2 p(x, y) = -Q_s \delta(x - x_s)\delta(y - y_s), \quad (1)$$

where ∇^2 is the two-dimensional Laplace operator, k is the wave number, $p(x, y)$ is the sound pressure at location (x, y), and Q_s is the source strength per unit length. In order to evaluate the sound pressure, the following boundary conditions should be satisfied:

(1) In the infinite far field ($\rho = \sqrt{x^2 + y^2} \to \infty$)

$$\lim_{\rho \to \infty} \sqrt{\rho}\left(\frac{\partial \rho(\rho, \theta)}{\partial \rho} - jkp(\rho, \theta)\right)$$
$$= 0 \text{ (Sommerfild radiation condition)}. \quad (2)$$

(2) At the boundaries

$$\begin{cases} \dfrac{\partial p(x, y)}{\partial n} = 0, \text{(for rigid boundry)} \\ \dfrac{\partial p(x, y)}{\partial n} = -j\omega\rho_0 v(x, y)Z(x, y)\text{(for absorptive boundary)}, \end{cases}$$
$$(3)$$

where $v(x, y)$ and $Z(x, y)$ are the particle velocity and specific acoustic impedance.

The sound wave equation and the associated boundary conditions can be solved using the standard BEM.[16] Upon solving the sound pressure response to the source excitation, the performance of the sound barrier is evaluated in terms of the IL

$$\text{IL} = 20 \log_{10}\left(\frac{|p_0|}{|p_1|}\right) \text{(dB)}, \quad (4)$$

where p_0 and p_1 are the sound pressure at the receiver location before and after the installation of the sound barrier, respectively. As the work presented here aims to study the performance of a WTB, no effort is being made to improve the algorithm of the BEM. Thus, the simulation is performed by employing the commercial software package SYSNOISE,[29] the software of which is found to be an effective tool for examining the barrier performance.[30]
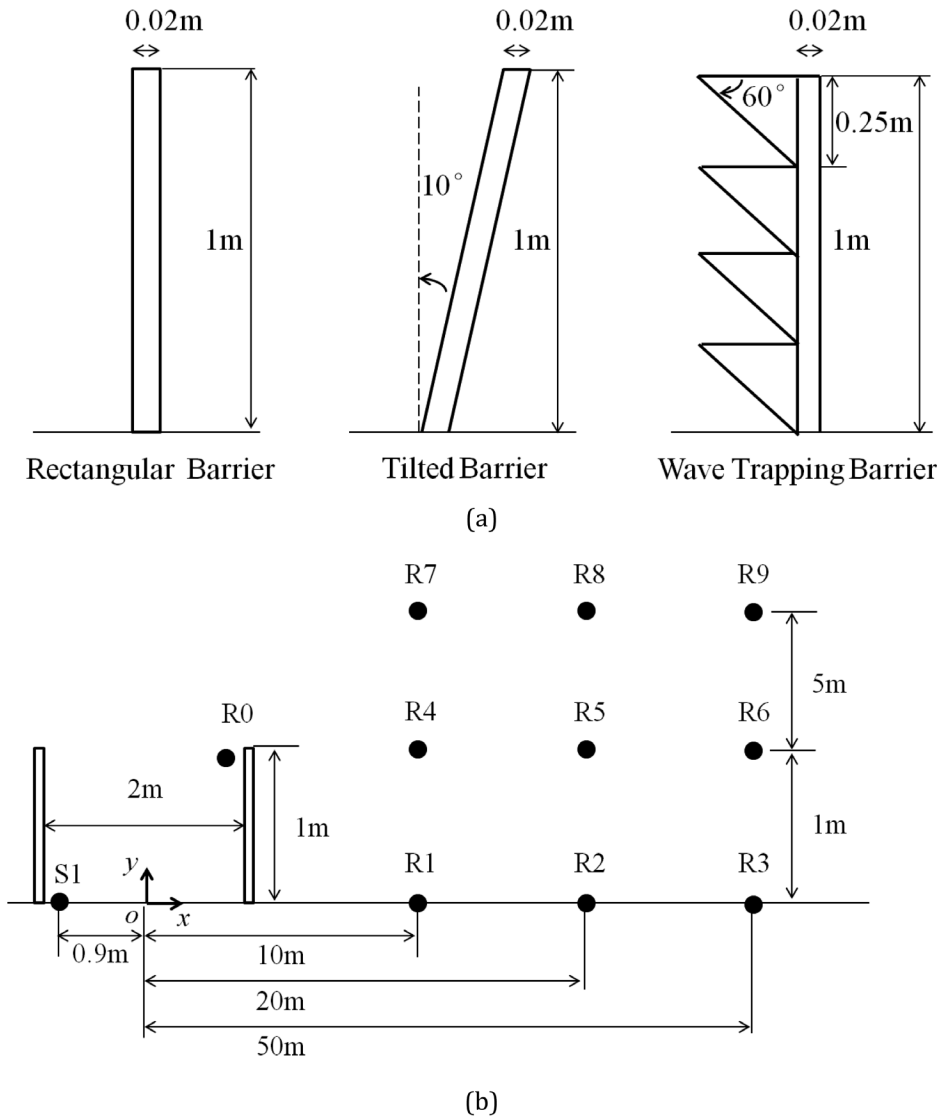
FIG. 1. Schematic diagrams of the investigated model: (a) Barriers of different profiles and (b) layout of barrier and measurement points.

III. RESONANCES WITHIN THE BOUNDED DOMAIN

The first topic to be studied is the deterioration of the performance of a conventional rectangular barrier when a reflecting wall of the same height is placed on the source side. For simplicity, the boundary conditions of the barrier and ground surfaces are assumed to be rigid. The dimensions of the sound barriers used for the analysis are shown in Fig. 1(a), with the locations of source ($S1$), receiver ($R1$), and reflecting wall drawn in Fig. 1(b). Location $R0$ is used to assess the strength of the sound field near the diffracting point. Locations $R2$ to $R9$ are evaluating points used for subsequent examination of the changes in the sound field when various barrier profiles are used.

The deterioration of the barrier performance due to the reflecting wall is examined by comparing the ILs of the rectangular barrier with and without the reflecting wall in Fig. 2. When the reflecting wall exists, a significant change in IL is observed. The barrier performance is improved at some frequencies, but at many other frequencies the performance degenerates. In particular, negative IL values are found. They indicate an increased sound pressure at receiver $R1$ due to the presence of the reflecting wall. Moreover, the IL curve

for the barrier with a reflecting wall displays intense fluctuations with many peaks and dips. This is a result of the constructive and destructive interference of direct and reflecting
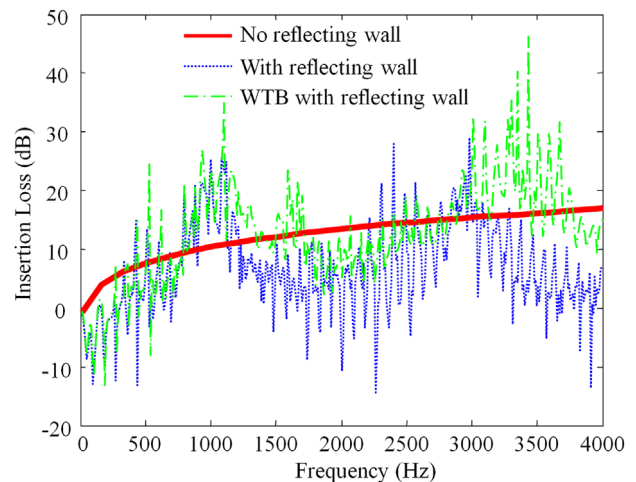

FIG. 2. (Color online) ILs observed at $R1$ for three configurations: A rectangular barrier without a reflecting wall, a rectangular barrier with a reflecting wall, and a WTB with a reflecting wall.

waves at the diffracting point, which is the barrier top according to the GTD.[4]

For a better understanding of this interference, the sound pressure distributions at the frequencies of six of the dips in the IL curve (the dotted curve in Fig. 2) are presented in Fig. 3. The dips are chosen because they correspond to the reduced performance in a "local" frequency range. It is noted that dips selected are just examples and the phenomenon applies to other dips as well. At each frequency, a clear spatial modal distribution is identified within the domain bounded by the reflecting wall and the barrier[31] (the domain is called the bounded domain hereafter). When the reflecting wall is placed opposite the barrier, multiple reflections occur at the surfaces of the reflecting wall and barrier, and these reflecting waves superimpose with each other and with the direct waves generated directly by the noise source. Under a harmonic excitation of the source, the constructive superposition of these waves forms a resonance response at resonance frequencies. Eventually, the sound pressure distribution at each of the above frequencies is dominated by one mode with its natural frequency closely coinciding with the frequency of the IL dip.

As will be illustrated in Sec. IV A, these modes can be classified as trapped modes. Trapped modes in an infinite space with local geometrical or material variations have been identified in many systems. For example, a fluid bounded by fixed surfaces and by a free surface of infinite extent is capable of localized modal vibration under gravity[32] (called a trapping mode). A unique characteristic of the trapped mode is that most of its acoustical energy is trapped in a local area, and the energy density decays with distance.

IV. TRAPPED MODES

A. Solution of the trapped modes

Mathematically, trapped modes are the eigensolutions of the homogeneous Helmholtz equation with specific boundary and joined conditions. Koch,[33] gave a numerical examination of the trapped modes in an open cavity. To solve the trapped modes under the configuration in Fig. 1(b), the commercial software COMSOL Multiphysics™ 3.5a is employed.[34] A basic difficulty in numerically solving the trapped modes is the radiation of sound waves to infinity.

Practically, the infinite domain has to be truncated to a relative small size domain for computing efficiency. But this treatment, in turn, causes unphysical wave reflections from the boundary. With this in mind, Perfectly Matched Layer (PML) absorbing boundary conditions[35] are employed. A PML enables an outgoing wave to leave the modeling domain with minimal reflections, promising the least influence on the domain of interest from the reflections. In the current analysis, PML is applied at the boundary of the original domain. A detail setup of this boundary condition can be referred to Koch's work.

The first six trapped modes of the current configuration are calculated and presented in Fig. 4 (the PML domain is not shown). As the characteristics of the trapped mode shows, a strong oscillation with a high pressure amplitude traps high energy within the bounded domain. In the region outside the domain, the amplitude decays with distance. It is worth noting that the resonant features of the trapped modes are also extended to the region outside the barrier and the reflecting surface. This is because the open configuration cannot trap all the energy within the bounded domain, which results in a pressure residue outside the bounded domain.

The orthogonal property of the trapped modes is also examined in a numerical way. This was done by integrating the product of any two modes in the domain divided by the domain area. It is found that the self-product terms are much larger than the cross-coupling terms, and the former are approximately constant. This indicates a good orthogonal property of the trapped modes.

B. Resonance frequencies of the trapped modes

The pressure distributions of the trapped modes in Fig. 4 between the barrier and the reflecting wall in the *x*-direction are similar to those of the (1,0), (2,0), (3,0), (4,0), (5,0), and (6,0) modes of a closed rigid-walled rectangular cavity of the same length in the *x*-direction. Although the rigid-walled boundary condition on the ground surface still produces a sound field similar to those of the (1,0) to (6,0) modes near the ground surface, the sound pressure distributions near the top opening are significantly different from those of the rigid wall modes, due to the radiation at the opening and diffraction by the barrier and reflecting wall. The radiation at the cavity opening also causes the resonances of the trapped
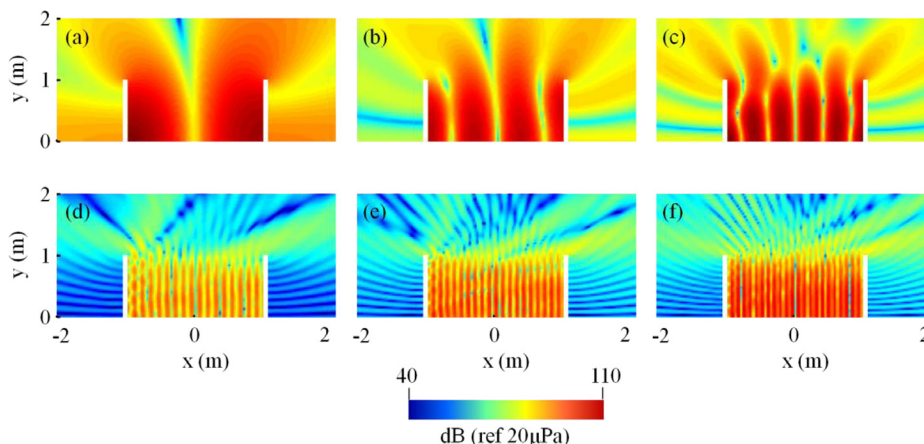

FIG. 3. (Color online) Sound pressure distributions at six dips of the IL curve (see dotted curve, Fig. 2) when a reflecting wall is placed opposite the rectangular barrier, for: (a) 100 Hz, (b) 270 Hz, (c) 440 Hz, (d) 1480 Hz, (e) 1740 Hz, and (f) 2000 Hz.
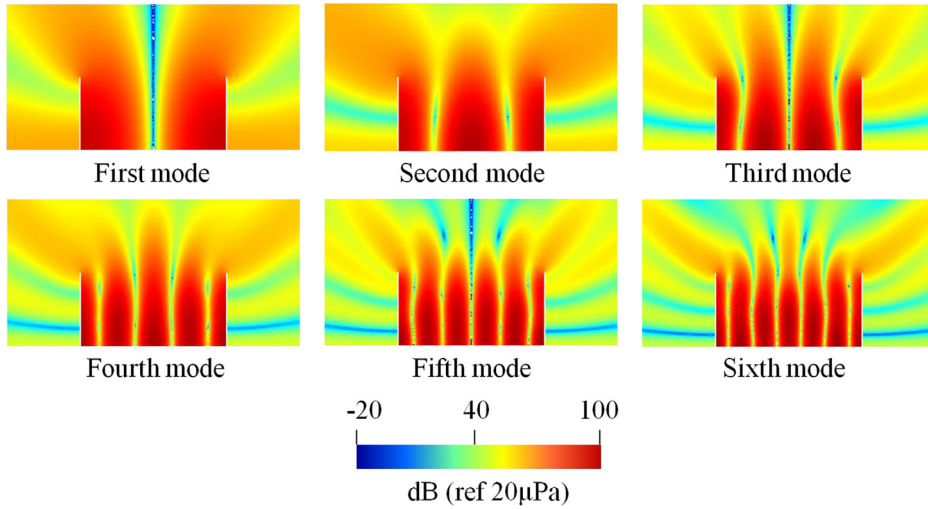
J. Acoust. Soc. Am., Vol. 134, No. 3, September 2013

Yang *et al.*: The wave-trapping barrier   1963

FIG. 4. (Color online) The first six trapped modes in the parallel barrier configuration.

First mode   Second mode   Third mode

Fourth mode   Fifth mode   Sixth mode

-20   40   100

dB (ref 20μPa)

modes to deviate from the resonances of the fully rigid cavity modes. For a rectangular cavity with all the boundaries rigid, the resonance frequencies of the horizontal modes (with modal structures parallel to the ground) are well known:

$$f_{(n,0)} = nc_0/2L, \qquad (5)$$

where n is the horizontal mode index, c_0 is the speed of sound, and L is the horizontal length of the cavity. A comparison shows that the resonance frequencies of the fully rigid cavity are slightly lower than those of the trapped modes. Indeed, unlike the cavity with all boundaries rigid, the barrier and reflecting wall bounded domain has the top boundary open. In this case, the surface mass at the opening becomes a finite value instead of an infinite one as it would be for a rigid top surface. As a result, the decreased boundary inertia causes the increase in the resonance frequencies of the trapped modes.

C. Sound pressure at the resonance frequencies of the trapped modes

The question of whether the trapped modes can completely represent the sound pressure field at all frequencies and locations remains an open question for further research. For a resonant system, the resonant modes often play a dominant role in describing the field response when the excitation frequency ω is equal to the resonance frequency ω_n of the system. For this case, the sound pressure response at r_o to a point source excitation at r_s can be approximately expressed as (see detailed derivation in the appendix)[36]

$$p(r_0, \omega_n) \approx \frac{c_0^2}{\Lambda_{nn}} \frac{Q_s \varphi_n(r_s)\varphi_n(r_0)}{2j\zeta_n\omega_n^2}$$
$$+ \sum_{m \neq n} \frac{c_0^2}{\Lambda_{mm}} \frac{Q_s \varphi_m(r_s)\varphi_m(r_0)}{(\omega_m^2 - \omega_n^2 + 2j\zeta_n\omega_n\omega_m)}, \qquad (6)$$

where φ_n and ζ_n are, respectively, the shape and damping ratio of the nth trapped mode. The second term in Eq. (6) is the contribution of other trapped modes with resonance

frequencies ω_m in the vicinity of ω_n. This non-resonance term becomes important when the source is located near the nodal point of the nth mode and/or when the observation location is located near the nodal point of the nth mode.

Using Eq. (6) and the characteristics of the trapped modes, the sound pressure at $R1$ is computed at the first 14 resonance frequencies and compared with the result obtained from SYSNOISE.

A total of 19 trapped modes (the eigenvalues of the trapped modes are listed in Table I) are used in Eq. (6) and below 800 Hz. The resultant sound pressures are marked as stars in Fig. 5. As Fig. 5 shows, the contribution of trapped modes dominates the radiated sound field at the resonance frequencies of the modes. In fact, these major peaks are only contributed to by the (*, 0) modes (The modal index are defined through visual inspection). Therefore, if research is only focused on predicting the major sound pressure peaks, the use of the (*, 0) modes is sufficient for a good prediction.

V. SOUND FIELD AT THE DIFFRACTING POINT

For a rigid barrier placed on a rigid ground surface, the energy generated by the sound source can only escape from the opening of the cavity. Since only the diffracted waves

TABLE I. The eigenvalues of the modes used in the modal superposition method to approximate the corresponding peak.

| Peak frequency (Hz)	Eigenvalues of the contributing modes	Peak frequency (Hz)	Eigenvalues of the contributing modes
50	64.14 + 6.13i	526	525.30 + 1.17i
102	103.49 + 3.66i	562 (weak)	561.43 + 10.25i
			602.90 + 14.28i
186	184.97 + 3.78i	610	611.87 + 0.92589i
270	267.63 + 1.86i	642 (weak)	644.01 + 9.91i
354	344.70 + 19.15i	698	699.52 + 1.03i
	353.15 + 2.06i		
440	438.86 + 1.34i	730 (weak)	730.29 + 8.48i
			745.05 + 19.61i
			759.99 + 12.60i
478 (weak)	482.29 + 13.89i	782	788.01 + 1.01i
	515.78 + 16.06i		
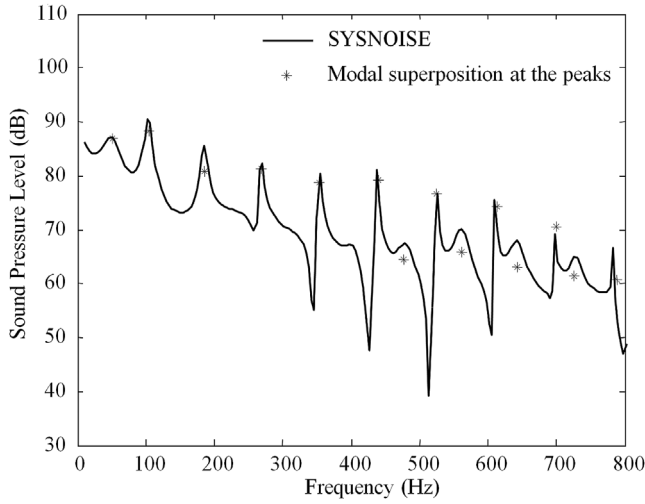
FIG. 5. Comparison of sound pressure levels at the receiving point, as calculated by SYSNOISE and by the modal superposition method.

FIG. 6. Diffraction coefficient D versus incident angle α at three different frequencies.

propagate into the shadow zone, the sound field properties around the opening region must be responsible for the efficiency of the diffraction and thus the sound pressure at the receiver's location in the shadow zone.

By analogy with the reflection and transmission coefficients defined for reflecting and transmitting waves, a diffraction coefficient D is suggested in the GTD.[4] In this definition, a diffraction field is determined by the acoustical property of the sound field at the diffracting point and D

$$p_d = D p_i r^{-1/2} e^{jkr}, \tag{7}$$

where p_d and p_i are, respectively, the sound pressure at the receiving and diffracting points, and r is the distance from the diffracting point to the receiving point. Equation (7) illustrates that: If a barrier is placed between the source and the receiver, the sound field at the receiving point is indirectly influenced by the incident wave. That is, the incident wave first approaches the barrier top and diffraction happens. The sound field at the barrier top then becomes a secondary source, generating diffracting waves. To this end, the sound pressure at the receiving point in the shadow zone has an inherent relationship with the sound pressure at the diffracting point. In addition, since the thickness of the barrier used in the current analysis is 0.02 m, which is much smaller than the wavelength of the frequency of interest, one could simply assume that the diffracting point is at the barrier top.

The diffraction coefficient D is determined by the directions of the incident and diffracting rays, the wavelength, and the geometrical and physical properties of the media at the point of diffraction. An asymptotical expanded form of the diffraction coefficient D is[4]

$$D = -\frac{e^{j\pi/4}}{2(2\pi k)^{1/2}} \left[\sec\left(\frac{\alpha - \theta}{2}\right) + \sec\left(\frac{\alpha + \theta}{2}\right) \right], \tag{8}$$

where α and θ are the angles as indicated in the enlarged view in Fig. 6.

For the configuration of barrier and receiving point $R1$ used in Fig. 1, the variation of the diffraction coefficient D
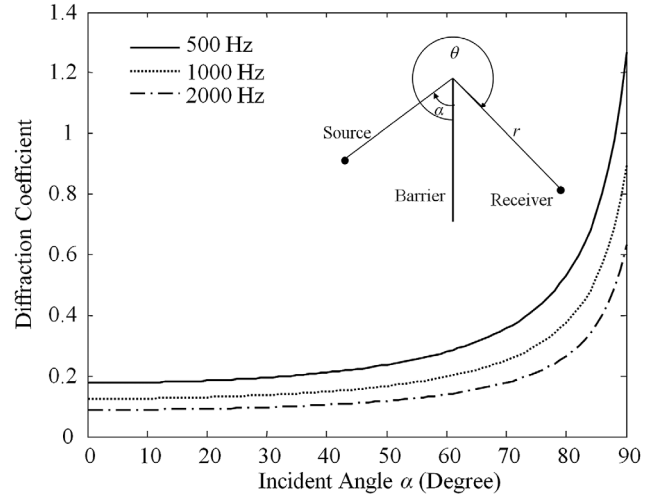
with respect to the incident angle α is plotted in Fig. 6 at different frequencies. As we are only interested in the states at and before diffraction happen, the distance r between the diffracting point (screen tip) and the receiver is fixed. The plots show that the diffraction coefficient is low for a high frequency. This implies that a sound wave with a small wavelength is diffracted with a low efficiency. As a result, the sound pressure at receiver $R1$ has a descending trend with the increase of frequency and the IL has an ascending trend. In addition, at the same frequency, the increase of α attains a bigger diffraction coefficient. That is to say, the sound wave is more effectively diffracted if the incident wave impinges normally to the barrier surface. In that case, the maximum diffraction coefficient is reached. If the incident wave is in parallel (at a grazing angle) with the barrier surface, a minimum diffraction coefficient is obtained. For instance, at 500 Hz, a maximum difference of 16 dB is made at receiver $R1$ if the sound wave direction varies from $0°$ to $90°$ at the diffracting point.

Attention is then paid to the sound intensity field in the region around the diffracting point. In Fig. 7, the sound intensity field is examined at a peak (510 Hz) and a dip (530 Hz) in the IL curve (the dotted curve in Fig. 2). At 510 Hz, the direction of the sound intensity field is nearly grazing along the barrier surface, in which case the diffraction coefficient D is minimized. At 530 Hz, the direction of the sound intensity field is nearly normal to the barrier surface and a maximum diffraction coefficient is obtained. Moreover, the amplitude of sound intensity (in terms of arrow length) is high at the dip frequency and low at the peak frequency. As a consequence, the diffracting source strength is high at 530 Hz, and it conducts a high sound pressure at receiving point $R1$ and yields an IL dip, and vice versa. As the IL curve in Fig. 2 predicts, an IL difference of 17 dB is found between these two frequencies.

The above analysis indicates the dominant role of resonance in deteriorating the barrier performance. This is further evidenced by examining the sound intensity and its direction at point $R0$ (at coordinates [0.9, 0.9]) in Fig. 8, a point that is quite close to the diffracting point in the
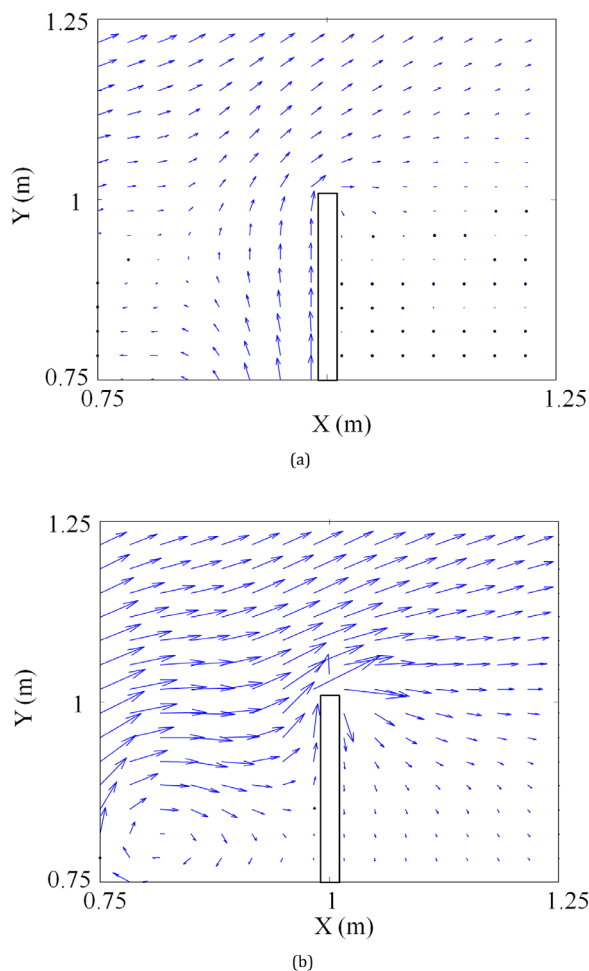
(a)

(b)

FIG. 7. (Color online) Sound intensity fields in the region around the diffraction point of the rectangular barrier, for (a) 510 Hz (IL peak) and (b) 530 Hz (IL dip).

configuration of Fig. 1(b). The resulting curves display intense fluctuations in the spectrum due to the dominating effect of each trapped mode. At the resonance of each mode, sound intensity is high and energy flux is moving perpendicular to the barrier surface, the conditions of which fulfill the
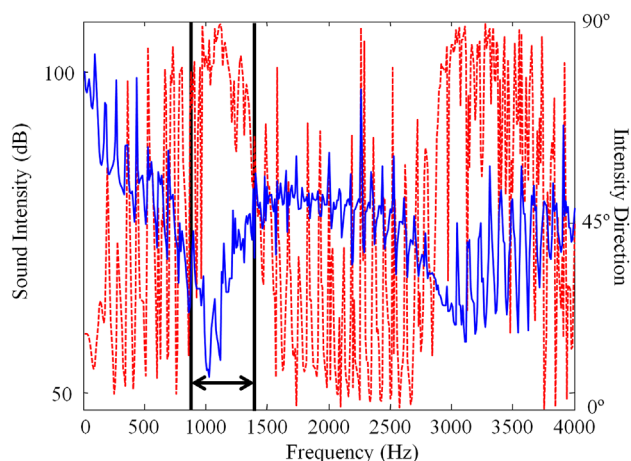

FIG. 8. (Color online) Sound intensity (solid) and its direction (dashed) at point R0. The marked region shows that the source is located at the nodal line of the trapped modes that are dominant around these frequencies, so the resonance effect is weak.

requirements of effective diffraction and thus barrier performance is degraded. Meanwhile, one may notice that within the spectrum between 900 and 1200 Hz that sound intensity decreases and has a big trough, implying a weak resonance effect in this spectrum. A plausible explanation is that the noise source is located at the nodal line of the modes that are dominant at these frequencies, so that the dominating modes are not well excited.

VI. WTB PERFORMANCE ANALYSIS

A. Rigid boundary conditions

The performance of the WTB is evaluated herein. As an illustration, the rectangular barrier is replaced by a WTB [the WTB profile is shown in Fig. 1(a)]. In order to have an overall evaluation of barrier performance, a mean IL is defined as

$$\text{IL}_{\text{mean}} = \frac{\sum_{i=1}^{N} \text{IL}(f_i)}{N}. \tag{9}$$

In Eq. (9), N is the total number of sampling frequencies used to calculate the total IL over the interested frequency range. The IL of this new profile is also predicted at $R1$ and compared with others in Fig. 2. When the WTB is used, the overall IL is improved due to the modified profile. In terms of IL_{mean}, the WTB obtains a 12.9 dB reduction, which is 4.7 dB higher than that of the rectangular barrier. However, one may notice that this improvement mainly occurs for a frequency above 1000 Hz. At a frequency below 1000 Hz, both barriers give nearly the same performance.

The change of barrier profile affects the mode shape of the trapped mode, and thus alters the sound field at the diffracting source. In this regard, the sound pressure distributions at 280 and 1730 Hz are examined and plotted in Figs. 9(a) and 9(b).

In Fig. 9(a), a similar pressure distribution to the ones in the rectangular barrier case is observed. At this frequency, the dominating mode is not significantly influenced due to the change of barrier profile. Therefore, the pressure distribution is unchanged and the contribution from this mode remains high. Consequently, the resonance effect still counts and degrades barrier performance. This explains the reason why no improvement is found at the frequency below 1000 Hz although WTB is used. At 1730 Hz which is above 1000 Hz, pressure distribution within the bounded domain is very diffuse. In terms of wavelength, 1730 Hz has a wavelength smaller than the size of the wedges on the WTB. Sound wave with wavelength less than this size is more sensitive to the change of barrier profile. For a wavelength within that length scale, the dominating modes are more easily affected by the change of barrier profile, and the influence occurs in terms of sound pressure redistribution. As a result, the sound pressure distribution at this frequency is very diffuse, and the resonance feature is hard to identify.

The redistribution of sound pressure alters the sound field around the diffracting source, and hence affects barrier performance. With this concern, the sound intensity field is examined at the WTB IL dips in Fig. 10. At 280 Hz in Fig. 10(a),
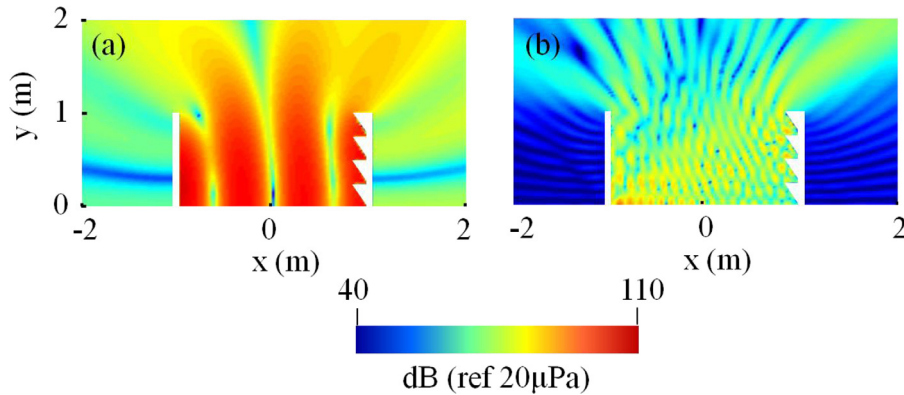
FIG. 9. (Color online) Sound pressure distributions at two dips of the IL curve when a reflecting wall is placed opposite the WTB: (a) 280 Hz and (b) 1730 Hz.

energy flux is moving from left to right, having the same flow pattern as it does in the IL dip in the rectangular case. Since the dominating mode at this frequency is unchanged or less affected by the change of barrier geometry, the sound intensity pattern remains the same. At 1730 Hz, however, the WTB takes effect. As can be observed in Fig. 10(b), energy flux is distorted and trapped around the wedge, which shows an obviously different flow pattern.

The variation happens as a consequence of the changed pressure distribution due to the WTB and the change manifests itself in terms of energy flux direction and intensity strength. At this frequency, the affected dominating mode redirects energy flow, so the energy flux is not moving perpendicular to the barrier surface. In this case, the diffraction coefficient D at the diffracting point becomes smaller. On the other hand, the strength of the diffracting source is also affected by the change of barrier profile, which causes less energy to be emitted after the diffracting point. To this end, the emitted energy is defined by integrating the sound intensity at the barrier top from the exterior barrier surface over $90°$ in an anticlockwise direction (i.e., from $\theta = 360°$ to $\theta = 270°$ in Fig. 6). The emitted energy of the rectangular barrier and the WTB are computed and compared in Fig. 11. Figure 11 shows, below 1000 Hz, that roughly the same amount of energy is emitted from the two barriers, which corresponds to the similar IL reductions in Fig. 2. Above 1000 Hz, the WTB emits less energy than a rectangular barrier, which corresponds to a better performance in Fig. 2.

B. Absorptive boundary condition

The second parameter that affects the diffraction source is the surface absorption of the barrier. It is found that the use of absorption on the boundary with different absorption coefficient values only influences the extent of the fluctuation of the IL curves, but the overall IL trend maintains the same. That is, a low absorption coefficient results in a fierce fluctuation while a high absorption value yields a moderate
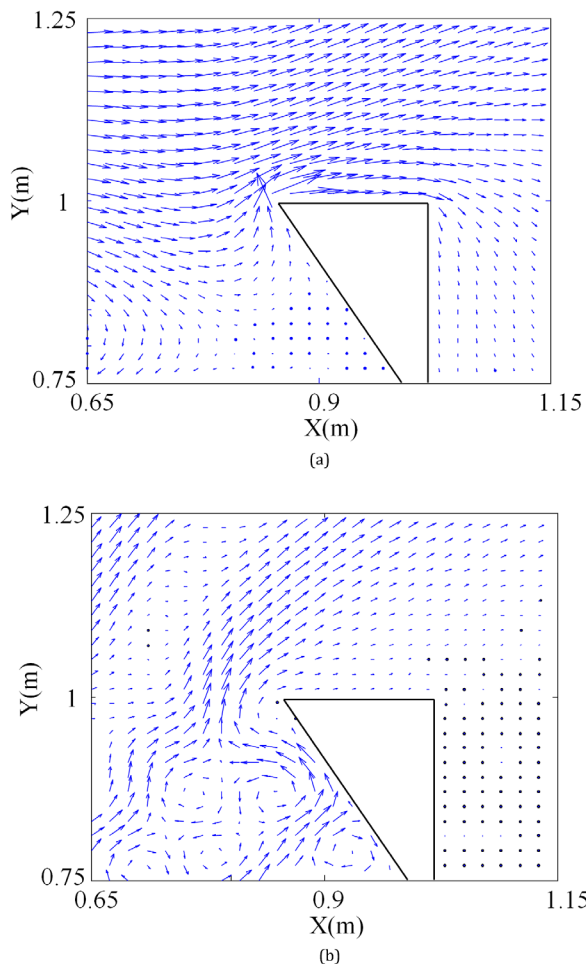

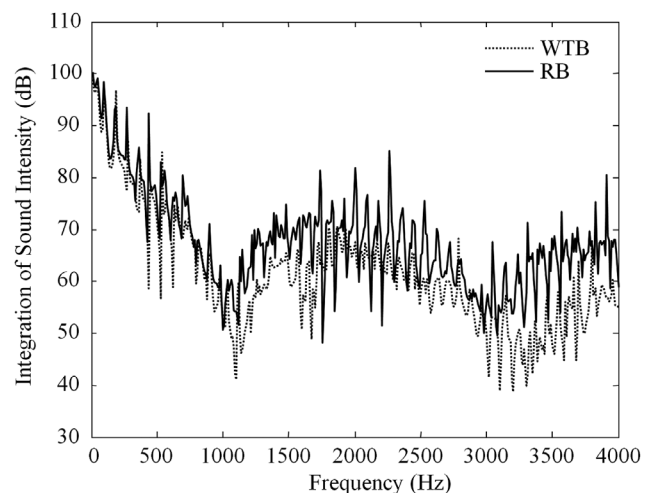FIG. 10. (Color online) Sound intensity field in the region around the diffraction point of the WTB, for: (a) 280 Hz (an IL dip) and (b) 1730 Hz (an IL dip).

FIG. 11. Integrations of the sound intensities of the rectangular barrier and the WTB.

TABLE II. IL$_{mean}$ of barrier with different profiles.

	Rectangular barrier (dB)	Tilted barrier (dB)	WTB (dB)
$R1$	7.2	11.8	13.2
$R2$	6.2	11.3	12.4
$R3$	5.5	10.9	11.9
$R4$	10.7	16.0	17.3
$R5$	10.1	15.2	16.8
$R6$	10.5	15.9	17.1
$R7$ (Illuminated zone)	3.2	2.0	3.8
$R8$	4.5	7.4	10.6
$R9$	7.8	13.7	14.7

fluctuation. The overall trends however maintain the same. In fact, the effect of the absorbent WTB surface is to reduce the strength of the sound waves reflecting from it. These waves superimpose with the waves coming to the reflecting wall, and generate the resonance effect (the standing wave effect) within the bounded domain. Since the strength of the wave is reduced, the resonance effect decreases as well. As a result, IL fluctuations that are dominated by the trapped modes become moderate.

VII. COMPARISON OF WTB TO RECTANGULAR BARRIER AND TILTED BARRIERS

The performance of the WTB is evaluated and compared with the conventional rectangular barrier and the tilted barrier with an angle of $10°$ that was suggested by Monazzam and Fard.[21] The dimensions of the barriers are drawn in Fig. 1(a). Comparisons are conducted at the nine receivers shown in Fig. 1(b) and the results are listed in Table II.

The results show that the tilted barrier has a better performance than that of the rectangular barrier in the shadow zone. When the WTB is used, a further average improvement of 1.6 dB is obtained. This shows the potential of the WTB as a solution to the performance deterioration when a reflecting wall is placed on the opposite side of the barrier. In the illuminated zone ($R7$), the tilted barrier has the worst performance. Meanwhile, the IL of the WTB is still better than that of the conventional rectangular barrier. Since the main function of the WTB is to reduce the effects of multiple reflections, it is not effective at reducing sound waves that are directly propagating to the receiver in the illuminated zone.

VIII. CONCLUSIONS

The deterioration of the IL of a conventional sound barrier with a large reflecting surface on the source side is due to the resonance response of the sound field to the source in the vicinity of the barrier and the reflecting surface. Such resonance is a feature of the trapped modes inherent in the parallel barrier configuration, the modes of which can be used to reproduce the sound field at any point in the domain by using the modal superposition method. At each resonance frequency, strong oscillations and high energy are trapped within the bounded domain. The high energy flux impinges normally on the barrier surface at the top, which is the most

effective diffraction condition based on the geometrical theory of diffraction. This results in the reduced IL.

A WTB for reducing this performance deterioration was studied in this paper. It was demonstrated that a WTB is effective in reducing this deterioration at frequencies where the wavelength of sound is comparable to or smaller than the dimensions of the wedges on its surface. The surface profile of the WTB reorganizes the pressure distribution within the bounded domain and alters the sound field at the diffracting point. This allows for a reduction of sound pressure at the receiver point. If absorptivity is further added to the surface of the WTB, the IL fluctuations governed by the resonance effect become moderate. However, the overall IL trend does not have a significant change. Finally, the performance of a WTB was compared with a conventional rectangular barrier and a tilted barrier. Results showed that the WTB has a better overall performance in IL.

APPENDIX

This appendix presents the derivation of Eq. (6). The sound radiation by the acoustic sources within the parallel barriers (also called an open resonator in previous work[37]) can be described by the eigenvalues k_n and the eigenfunctions $\phi_n(x, y)$, described by a boundary value problem of the Helmholtz equation. For this problem, the two-dimensional Helmholtz equation needs to be solved subject to Neumann boundary conditions on the rigid surfaces of the ground and the sound barriers, allowing only outgoing waves with a positive outward flow of sound energy. The eigensolutions satisfy the Helmholtz equation

$$\nabla^2 \phi_n(x, y) = -K_n^2 \phi_n(x, y). \tag{A1}$$

Due to the radiation loss of the outgoing waves, the eigenvalues are complex, with $\mathrm{Re}(K_n)$ producing the resonance frequencies ($\omega_n = c_0 \, \mathrm{Re}(K_n)$) and both it and $\mathrm{Im}(K_n)$ determining the quality factors of the resonance modes ($Q_n = \mathrm{Re}(K_n)/2|\mathrm{Im}(K_n)|$). The modal damping ratio and quality factor are related by $\zeta_n = 1/2Q_n$. As a result, $K_n = \omega_n/c_0(1 + j\zeta_n)$.

The sound pressure generated by a point source within the open resonator is expanded by the eigenfunctions

$$p = \sum_m p_m \phi_m(x, y), \tag{A2}$$

and then substituted into Eq. (1). Using Eq. (A1) and the orthogonality property of the eigenfunctions, the modal amplitude is obtained as

$$p_m = \frac{-Q_s \phi_m(x_s, y_s)}{\Lambda_{mm}(-K_m^2 + k^2)}, \tag{A3}$$

where $\Lambda_{mm} = \int_A \phi_m^2(x, y)\, dx dy$ and A is the domain in which the eigenvalues and eigenfunctions are calculated. Thus, for $\zeta_m \ll 1$, Eq. (A2) becomes

$$p(x, y, \omega) = \sum_m \frac{c_0^2 Q_s \phi_m(x_s, y_s)\phi_m(x, y)}{\Lambda_{mm}(\omega_m^2 - \omega^2 + j2\zeta_m \omega_m^2)}. \tag{A4}$$

The calculation of the eigenvalues and eigenfunctions demonstrates the existence of two types of modes. The first type includes the trapped modes, which have a small radiation loss, while the second type includes the leaky modes, which are associated with a large radiation loss. The high-frequency leaky modes are numerically difficult to determine. On the other hand, at frequencies located away from the resonance frequencies, or where the dominating trapped modes are not effectively excited by the source, a large number of leaky modes are required for an accurate description of the sound pressure. As a result, the accuracy of the modal expansion of the sound pressure will be poor at those frequencies.

However, the modal expansion will give a more accurate description of the sound pressure when the driving frequency is equal to one of the resonance frequencies of the trapped modes. This is because the trapped modes can be readily determined numerically and because it has a dominating magnitude if the sound field is excited at its resonance frequency and if the source and the corresponding eigenfunction are well coupled. For this case, Eq. (A4) can be approximated as

$$\begin{aligned}
p(r, \omega_n) \approx & \frac{c_0^2}{\Lambda_{nn}} \frac{Q_s \varphi_n(r_s)\varphi_n(r)}{2j\zeta_n \omega_n^2} \\
& + \sum_{m \neq n} \frac{c_0^2}{\Lambda_{mm}} \frac{Q_s \varphi_m(r_s)\varphi_m(r)}{(\omega_m^2 - \omega_n^2 + 2j\zeta_n \omega_n \omega_m)},
\end{aligned} \tag{A5}$$

where $r = (x, y)$ and $r_s = (x_s, y_s)$.

[1] S. I. Hayek, "Mathematical modeling of absorbent highway sound barriers," Appl. Acoust. **31**, 77–100 (1990).

[2] P. A. Morgan, D. C. Hothersall, and S. N. Chandler-Wilde, "Influence of shape and absorbing surface—A numerical study of railway sound barriers," J. Sound Vib. **217**, 405–417 (1998).

[3] S. K. Tang, "Noise screening effects of balconies on a building facade," J. Acoust. Soc. Am. **118**, 213–221 (2005).

[4] J. B. Keller, "Geometrical theory of diffraction," J. Opt. Soc. Am. **52**, 116–130 (1962).

[5] A. D. Pierce, "Diffraction of sound around corners and over wide barriers," J. Acoust. Soc. Am. **55**, 941–955 (1973).

[6] Z. Maekawa, "Noise reduction by screens," Appl. Acoust. **1**, 157–173 (1968).

[7] I. Ekici and H. Bougdah, "A review of research on environmental sound barriers," Build. Acoust. **10**, 289–323 (2003).

[8] K. M. Li and H. Y. Wong, "A review of commonly used analytical and empirical formulae for predicting sound diffracted by a thin screen," Appl. Acoust. **66**, 45–76 (2005).

[9] D. N. May and M. M. Osman, "Highway sound barriers: New shapes," J. Sound Vib. **71**, 73–101 (1980).

[10] T. Ishizuka and K. Fujiwara, "Performance of sound barriers with various edge shapes and acoustical conditions," Appl. Acoust. **65**, 125–141 (2004).

[11] D. Duhamel, "Shape optimization of sound barriers using genetic algorithms," J. Sound Vib. **297**, 432–443 (2006).

[12] M. R. Monazzam and P. Nassiri, "Performance of profiled vertical reflective parallel sound barriers with quadratic residue diffusers," Int. J. Environ. Res. **3**, 69–84 (2009).

[13] R. Seznec, "Diffraction of sound around barriers: use of the boundary elements technique," J. Sound Vib. **73**, 195–209 (1980).

[14] D. C. Hothersall, S. N. Chandler-Wilde, and M. N. Hajmirzae, "Efficiency of single sound barriers," J. Sound Vib. **146**, 303–322 (1991).

[15] L. A. de Lacerda, L. C. Wrobel, H. Power, and W. J. Mansur, "A novel boundary integral formulation for three-dimensional analysis of thin acoustic barriers over an impedance plane," J. Acoust. Soc. Am. **104**, 671–678 (1998).

[16] T. W. Wu, *Boundary Element Acoustics: Fundamentals and Computer Codes* (Cambridge WIT Press, Southampton, 2000), Chaps. 2 and 3.

[17] B. E. Treeby and J. Pan, "A practical examination of the errors arising in the direct collocation boundary element method for acoustic scattering," Eng. Anal. Boundary Elem. **33**, 1302–1315 (2009).

[18] W. Bowlby and L. F. Cohn, "A model for insertion loss degradation for parallel highway sound barriers," J. Acoust. Soc. Am. **80**, 855–868 (1986).

[19] G. R. Watts and N. S. Godfrey, "Effects on roadside noise levels of sound absorptive materials in sound barriers," Appl. Acoust. **58**, 385–402 (1999).

[20] G. R. Watts, "Acoustic performance of parallel traffic sound barriers," Appl. Acoust. **47**, 95–119 (1996).

[21] M. R. Monazzam and S. M. B. Fard, "Impacts of different median barrier shapes on a roadside environmental noise screen," J. Environ. Eng. Sci. **28**, 435–441 (2011).

[22] J. Pan, R. Ming, and J. Guo, "Wave trapping barriers," in *Proceedings of ACOUSTICS*, Gold Coast, Australia (2004), pp. 283–288.

[23] F. Fahy, D. G. Ramble, J. G. Walker, and M. Sugiura, "Development of a novel modular form of sound absorbent facing for traffic sound barriers," Appl. Acoust. **44**, 39–51 (1995).

[24] U. J. Kurze, "Noise reduction by barriers," J. Acoust. Soc. Am. **55**, 504–518 (1974).

[25] E. Rehoul, A. L. Bot, and J. P. Liaudet, "Radiative transfer equation for multiple diffraction," J. Acoust. Soc. Am. **118**, 1326–1334 (2005).

[26] H. S. Kim, J. S. Kim, H. J. Kang, B. K. Kim, and S. R. Kim, "Sound diffraction by multiple wedges and thin screens," Appl. Acoust. **66**, 1102–1119 (2005).

[27] H. Min and X. Qiu, "Multiple acoustic diffraction around rigid parallel wide barriers," J. Acoust. Soc. Am. **126** 179–186 (2009).

[28] P. Morse and K. Ingard, *Theoretical Acoustics* (McGraw-Hill, New York, 1968), Chaps. 9 and 10.

[29] *SYSNOISE User's Manual Rev. 5.5* (LMS International, Leuven, 2000), Chaps. 1–17.

[30] J. Lai, "Application of the Boundary Element Method to assessment of road traffic barriers," in *Proceedings of the 2nd SYSNOISE Users Meeting*, Leuven, Belgium (June 19–21, 1995).

[31] C. Yang, J. Pan, and L. Cheng, "Performance analysis of the wave trapping barrier," in *Proceedings of ACOUSTICS*, Fremantle, Australia (November 21–23, 2012).

[32] F. Ursell, "Trapping modes in the theory of surface waves," Math. Proc. Cambridge Philos. Soc. **55**, 941–955 (1951).

[33] W. Koch, "Acoustic resonances in rectangular open cavities," AIAA. J. **43**, 2342–2349 (2005).

[34] COMSOL Multiphysics, *Acoustics Module User's Guide* (COMSOL AB, Sweden, 2008), Chaps. 1–9.

[35] J. Berenger, "A perfectly matched layer for the absorption of electromagnetic waves," J. Comput. Phys. **114**, 185–200 (1994).

[36] J. Pan and D. A. Bies, "The effect of fluid-structural coupling on sound waves in an enclosure—Theoretical part," J. Acoust. Soc. Am. **87**, 691–707 (1990).

[37] S. Hein, W. Koch and L. Nannen, "Trapped modes and Fano resonances in two-dimensional acoustical duct-cavity systems," J. Fluid Mech. **692**, 257–287 (2012).